

## Colliding Clouds in the Milky Way’s Central Bar

SAVANNAH R. GRAMZE,<sup>1,2</sup> JUERGEN OTT,<sup>1,\*</sup> DAVID MEIER,<sup>3,1,\*</sup> BRIAN E. SVOBODA,<sup>1,†</sup> AND YANCY SHIRLEY<sup>2</sup>

<sup>1</sup>National Radio Astronomy Observatory, 1003 Lopezville Rd, Socorro, NM 87801 USA

<sup>2</sup>Steward Observatory, University of Arizona, 933 North Cherry Avenue, Tucson, AZ 85721

<sup>3</sup>New Mexico Institute of Mining and Technology, 801 Leroy Pl, Socorro, NM, 87801 USA

### ABSTRACT

We observed a cloud in the Galactic Center at (l,b) = (+5.4, -0.4) with ALMA and the ACA. We took measurements of the spectral lines <sup>12</sup>CO(2-1) (230.538 GHz), <sup>13</sup>CO(2-1) (220.368 GHz), C<sup>18</sup>O(2-1) (219.530 GHz), H<sub>2</sub>CO(3<sub>03</sub>-2<sub>02</sub>) (218.222 GHz), H<sub>2</sub>CO(3<sub>22</sub>-2<sub>21</sub>) (218.730 GHz), CH<sub>3</sub>OH (4<sub>22</sub>-3<sub>12</sub>) (218.440 GHz), OCS (18-17) and SiO(5-4) (217.075 GHz). We observed a velocity bridge, evidence of a cloud-cloud collision, between two clouds at  $\sim 50$  km s<sup>-1</sup> and  $\sim 150$  km s<sup>-1</sup> in our pv diagram. We found evidence of strong shocks due to the presence of SiO and weak shocks due to enhanced abundances of CH<sub>3</sub>OH. We believe that the  $\sim 50$  km s<sup>-1</sup> cloud came from gas which overshot the CMZ as it flowed in and that the cloud is colliding with the  $\sim 150$  km s<sup>-1</sup> cloud on the opposite side of the galaxy’s dust lane.

*Keywords:* ISM: clouds — ISM: molecules — ISM: structure — Galactic Center — astrochemistry

### 1. INTRODUCTION

The Milky Way is a barred spiral galaxy (Sormani et al. 2015). It has a central, elongated,  $\sim 2$ kpc radius bar with several spiral arms extending from it (Sormani et al. 2015). Material flows along the bar from the surrounding galaxy in the form of molecular clouds. As these clouds approach the Central Molecular Zone (CMZ) in the Galactic Center (GC), they heat up and become more turbulent (Morris & Serabyn 1996). Due to the gravitational bar potential, the molecular clouds orbit the GC along bar orbits, called X<sub>1</sub> orbits in literature (Morris & Serabyn 1996). The orbit’s innermost X<sub>1</sub> intersect themselves at the ends of their bar shape, where there are cusps (Sormani et al. 2015). Because of their self intersecting nature, molecular clouds on these orbits become shocked, lose angular momentum and fall in towards the CMZ. In some models, the CMZ is theorized to be X<sub>2</sub> orbits ensconced in and perpendicular to the middle of the larger X<sub>1</sub> orbits, fed by the gas falling from the X<sub>1</sub> orbits (Morris & Serabyn 1996).

In last summer’s NRAO REU project, two molecular clouds situated at point symmetric coordinates, Bania 1 (l,b) = (-5.4, +0.4) (Bania et al. 1986) and G5 (+5.4, -0.4) (Sormani et al. 2019), were studied with ALMA multi-line observations. Their coordinates are inverses of each other, giving credence to the idea that symmetric processes are happening on opposite sides of the galaxy which caused these two

clouds to be excited. Showing properties such as wide line widths and warm kinetic temperatures, these clouds are similar to other clouds found in the CMZ, despite being around five degrees in galactic longitude ( $\sim 1$  to  $\sim 2$  kpc away in Figure 14) away from the CMZ. These clouds might be evidence of gas inflow into the CMZ.

However, regardless of their symmetric coordinates, Bania 1 and G5 were found not to have identical properties. G5 is warmer than Bania 1, shows a strong velocity gradient that the other is lacking, and is more turbulent (Gramze et al. 2020). Kinetic gas models suggest that Bania 1 is either a view down one of the shock fronts along the X<sub>1</sub> orbits, or a cloud at the end of the galactic bar (Sormani et al. 2019). On the other side, G5 might be a collision point, where a molecular cloud overshot the CMZ and collided with another cloud flowing in from the other side, as modeled by Sormani et al. (2019).

The goal of this project in summer 2020 is to examine a newly observed part of G5, which completes the survey of this molecular cloud and the coverage of the observed ALMA project. A potential cloud interaction region exists within these new observations.

### 2. OBSERVATIONS

The ALMA Atacama Compact Array (ACA) was used to observe the molecular clouds B1 and G5. Both 7m and Total Power observations were made. The ACA was used as it is compact yet sensitive enough to observe the large structures of these clouds. The ACA is made up of four 12m antennas and twelve 7m antennas. It has a resolution of 6” in Band 6 (around 220 GHz), which was used to observe in the pertinent spectral lines. This resolution corresponds to structures about 0.25pc in size in the GC, 8.2kpc away. For the 12m

Corresponding author: Savannah R. Gramze  
sgramze@email.arizona.edu

\*

† Jansky Fellow of the National Radio Astronomy Observatory

total power telescopes, the resolution was  $30''$ , or physical size at the Galactic center of 1.25pc. Two rectangular fields-of-view were situated on top of the brightest regions of these two clouds to sample the most interesting parts of the clouds. A total of about 60 hours of time were distributed across the four regions. The spacing of each pointing was 0.7 times the size of each primary beam to optimize area sampled to the signal to noise ratio.

The correlator was setup includes several astronomically important spectral lines. The first are the isotopologues of carbon monoxide:  $^{12}\text{CO}$  (2-1) at rest frequency 230.538 GHz,  $^{13}\text{CO}$  (2-1) at rest frequency 220.368 GHz, and  $\text{C}^{18}\text{O}$  (2-1) at rest frequency 219.530 GHz. Isotopologues are molecules with one or more atoms replaced by their isotopes. The four weaker lines, which are  $\text{SiO}$  (5-4),  $\text{HC}_3\text{N}$  (24-23),  $\text{H}_2\text{CO}$  ( $3_{22-2_{21}}$ ) and  $\text{H}_2\text{CO}$  ( $3_{03-2_{02}}$ ) have the same  $320 \text{ km s}^{-1}$  bandwidth and  $0.7 \text{ km s}^{-1}$  channel width.  $\text{SiO}$  (5-4) at rest frequency 217.075 GHz is a strong shock tracer, which should help determine how turbulent these clouds are as a result of shocks, and  $\text{HC}_3\text{N}$  (24-23) (rest frequency 218.295 GHz) is an excitation tracer.  $\text{CH}_3\text{OH}$  ( $4_{22-3_{12}}$ ) at 218.440 GHz is a weak shock tracer, and shares a spectral window with  $\text{HC}_3\text{N}$  (24-23). The two formaldehyde lines,  $\text{H}_2\text{CO}$  ( $3_{03-2_{02}}$ ) (rest frequency 218.222 GHz) and  $\text{H}_2\text{CO}$  ( $3_{22-2_{21}}$ ) (rest frequency 218.730 GHz), can be used together as temperature tracers. Another line is the radio recombination transition  $\text{H}(30)\alpha$  at rest frequency 231.901 GHz, which has the largest bandwidth of 1875MHz or  $305 \text{ km s}^{-1}$  and a channel width of  $1.26 \text{ km s}^{-1}$  to capture the potentially wide recombination line.

### 3. METHODS

Only single dish total power (TP) data was used in the summer project. We received TP and 7m interferometric ACA spectral cubes imaged using the ALMA pipeline calibration and imaging. We checked the cubes over for errors that might interfere with the data. The most immediate defect in the data was an atmospheric feature present in the  $\text{H}(30)\alpha$  cube, which was so extreme that it drowned out any other spectral information from that line. Next, the rest frequencies of the spectral windows were checked to ensure that they matched those which were targeted. The relative velocities of notable spectral features were recorded.

In the spectral cube targeting a transition of  $\text{HC}_3\text{N}$ , no emission from  $\text{HC}_3\text{N}$  was found, but the cube did contain incomplete spectral information for  $\text{CH}_3\text{OH}$  ( $4_{22-3_{12}}$ ). The cube was recentered around that molecule's rest frequency, 218.440 GHz, using the CASA task `imreframe`.

#### 3.1. Baseline Ripple

Single dish data often suffers from unstable baselines, and the spectral cubes exhibited a baseline ripple, as seen in Figure 1. Baseline ripples originate from reflections off of the structure of the telescope from a bright radio source. These reflections cause a standing wave in the optics, which makes a sine wave appear in each spectrum. This issue is usually removed before imaging by fitting a polynomial to each

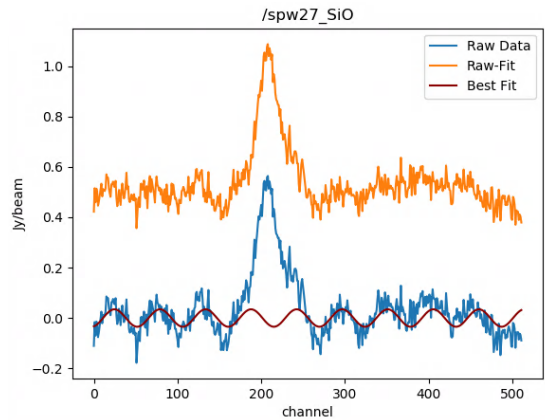


**Figure 1.** Plot of the process of fixing the baseline ripple. The raw spectrum being fit is on the bottom in blue. The red sine wave overlaid on top of it is the best fit to channels without emission. The orange spectrum above is the data with the best fit removed.

observed spectrum. However, we found that our data still showed residual ripples in the spectral cubes, see the blue spectrum in Figure 1. The baseline ripple was removed using the Python library `lmfit`<sup>1</sup> to create a best fit for the polynomial after averaging the cube spatially. Instead of a polynomial, we found that a sine wave was a better fit for the baseline issue, and we determined a best fit sine wave from channels without emission. The red wave in Figure 1 was the best fit for that cube. A single sine wave was all that was needed to remove the ripple, as the baseline ripple did not strongly vary spatially in the cubes. The orange spectrum in Figure 1 has the ripple removed. The best fit sine wave was then subtracted from each pixel.

While fixing the baseline ripple, an untargeted spectral line was found in one of the spectral windows. Since the feature was morphologically similar to that of the targeted molecule in that spectral window, as the shape of the features and their location on the field was similar, we assumed that they were at the same velocity. By comparing the frequency of this line with that of the corresponding emission from the line that was targeted and the rest frequency, we determined the molecular transition's rest frequency. That frequency was 218.904 GHz, corresponding to  $\text{OCS}$  (18-17), which was not previously identified in any of the fields of G5 or Bania 1.

#### 3.2. Image Combination

The new field from this year, G5a, is an extension of G5b from last year. Each spectral window was designed to have the same number of channels and same channel width for both fields. The two fields were combined by first using the CASA task `imregrid` to regrid the cubes to a wider field of view which contained the entirety of G5 in J2000 coordinates. Next, the CASA masks of the cubes were copied then removed using the `makemask` task. Then, the unmasked

<sup>1</sup> <https://lmfit.github.io/lmfit-py/index.html>

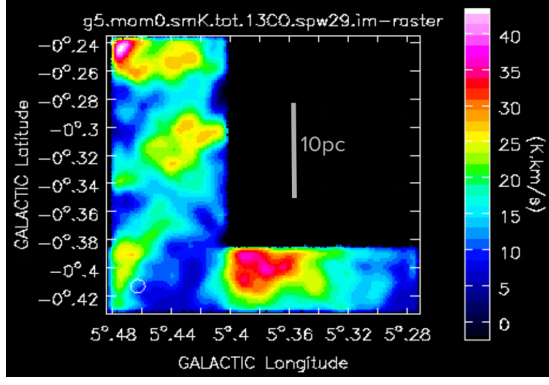


**Figure 2.** Combined integrated intensity map of  $^{13}\text{CO}$  (2-1) for G5a and G5b together.

cubes containing the same spectral windows were added together using the `immath` task. Their masks were added together separately, to make a weight map that also contained information about where the total combined field was contained. Using `immath`, the combined cube was divided by the combined mask, keeping only values of the mask higher than zero unmasked in the image cube produced. The product was then regridded using the `imregrid` task to be in galactic coordinates. Figure 2 is an example of the combined field.

### 3.3. Formaldehyde Kinetic Temperature

The kinetic temperature of the clouds was determined using a ratio between the  $\text{H}_2\text{CO}$  ( $3_{03}-2_{02}$ ) and  $\text{H}_2\text{CO}$  ( $3_{22}-2_{21}$ ) integrated intensity maps. For the ratio, only bright significant emission was included, so anything below 1 sigma of the noise was masked. The temperature of the clouds were determined separately to keep overlap emission from affecting the results. A second degree polynomial based on RADEX (van der Tak et al. 2007) data was used to relate the kinetic temperature of the  $\text{H}_2$  gas to the ratio between the two transitions (Ginsburg et al. 2016). From there, only the temperatures between about 25K to 80K were considered valid, as the approximation used to calculate them is not accurate for low temperatures and any gas above 80K is considered ‘hot.’ The method for finding the temperature used the polynomial:

$$T = 590 \times R_{\text{H}_2\text{CO}}^2 + 2.88 \times R_{\text{H}_2\text{CO}} + 23.4 \quad (1)$$

The temperatures of the two clouds were taken using separate integrated intensity maps for the two clouds, as the overlap in emission would be enough to throw off the results.

### 3.4. Opacity

Radiative transfer (LTE approx. motion) was used to constrain CO cloud opacity. Ratios of  $^{12}\text{CO}$  were made to each of its isotopologues. These ratios were used to calculate an initial estimate of the CO opacity of these clouds, and to derive the location and history of the gas by comparing them to GC values, 30 for  $^{12}\text{CO} / ^{13}\text{CO}$  and 200 for  $^{12}\text{CO} / \text{C}^{18}\text{O}$ . The variable  $\tau$  represents the opacity of the cloud, or how

transparent it is in that particular transition. By plotting the ratio versus  $\tau$  for the two isotropic ratio values of the isotopologues of CO, as in Figure 17, and comparing the ratios calculated by dividing the integrated intensity maps, the real  $\tau$  values can be approximated.

$$R_{1/2} = \frac{1 - e^{-\tau}}{1 - e^{-\frac{\tau}{A_2}}} \quad (2)$$

The  $\text{H}_2$  column densities of the clouds were calculated using the Strong et al. (1988)  $^{12}\text{CO}$  to  $\text{H}_2$  factor conversion. As that factor uses the (1-0) transition of  $^{12}\text{CO}$ , the integrated intensity map of  $^{12}\text{CO}(2-1)$  ( $M_{0_{12}\text{CO}(2-1)}$ ) was divided by 0.8 to account for the difference between the brightness of the two transitions.

$$N(\text{H}_2) = X \times \frac{M_{0_{12}\text{CO}(2-1)}}{0.8} \quad (3)$$

$$X = 2.3 \pm 3 \times 10^{12} \text{ cm}^{-2} (\text{K km s}^{-1})^{-1} \quad (4)$$

### 3.5. Shock Tracers

The column densities for the shock tracers SiO (5-4) and  $\text{CH}_3\text{OH}$  ( $4_{22}-3_{12}$ ) depend on the kinetic temperature of the clouds, which was determined using the formaldehyde line ratio. The general formula for the column density is in Figure 3 (Mangum & Shirley 2015).

$$N_{\text{tot}} = \frac{3h}{8\pi^3 |\mu_{ul}|^2 g_u} \exp\left(\frac{E_u}{kT_{\text{ex}}}\right) \left[ \exp\left(\frac{h\nu}{kT_{\text{ex}}}\right) - 1 \right]^{-1} \int \tau_\nu dv.$$

**Figure 3.** General equation for the total column density by Mangum & Shirley (2015).

The shock tracer abundance ratios were made by dividing the column density of the shock tracers by the column density of  $\text{H}_2$ .

Chemistry line intensity ratio maps were created by dividing the integrated intensity maps of the various molecules other than CO by the map of  $^{13}\text{CO}$  (2-1).

### 3.6. Slices

We determined that the G5a field contained two colliding clouds. The collision front between the two clouds is almost vertical in galactic latitude. To have a better signal to noise and to find the properties of the interface, we collapsed the galactic latitude axis and obtained a 1D slice along the galactic longitude axis for each of the individual molecule properties. We took horizontal slices of our maps to clearly show how properties of the clouds changed from one side of the maps to the other. There were three regions for these slices: the high velocity cloud on the left, the interface between the two clouds where they overlap and interact, and the right hand low velocity cloud. Slices were taken of the resulting maps by rebinning the images with the CASA task `imrebin`, which flattened them vertically. The line was then plotted. The interface plotted in grey was determined

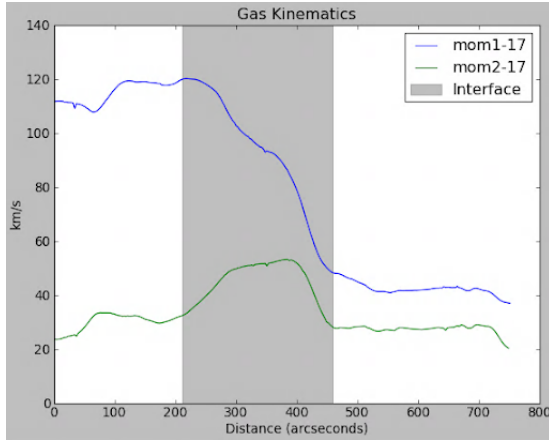


**Figure 4.** Plot of the slices of the velocity field (in blue) and velocity dispersion (in green) horizontally across galactic longitude. The interface is situated around the peak in velocity dispersion, where the two clouds are interacting.

using the width of the enhanced velocity dispersion where the two clouds overlap as seen in Figure 4, where we think the clouds are most likely interacting with each other.

#### 4. DISCUSSION AND RESULTS

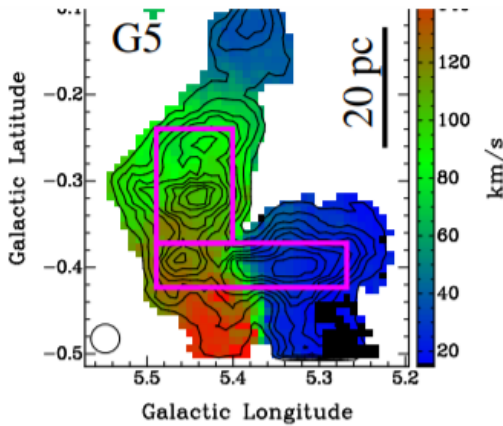


**Figure 5.** Velocity field of G5 in color with black integrated intensity contours on top from the  $\text{NH}_3$  (3,3) Mopra HOPS Survey (Purcell et al. 2012)(Longmore et al. 2017)(Walsh et al. 2011). The magenta rectangles are the rough outlines of the observed fields.

G5 is a giant molecular cloud, with its projection on the sky shaped like the letter L. Its projection is around 30pc tall and 40pc long. We observed an L-shaped region of G5, as outlined in magenta in Figure 5. We used the horizontal section of G5 (G5a) for this summer’s work. The vertical portion, studied last year, we dubbed G5b. G5a contains two wide spectral features in velocity space, one centered at  $\sim 50 \text{ km s}^{-1}$  and another at around  $\sim 150 \text{ km s}^{-1}$ . G5b has one wide spectral feature stretching from  $\sim 50 \text{ km s}^{-1}$  to  $\sim 150$

$\text{km s}^{-1}$ . The lower part of G5b extends down into the left side of G5a in Figure 5, overlapping slightly.

During the review of the data, it was found that the spectral cubes all contained two wide spectral features, molecular clouds, one at  $\sim 50 \text{ km s}^{-1}$  and the other at  $\sim 150 \text{ km s}^{-1}$ . At first, we speculated that the cloud at  $\sim 50 \text{ km s}^{-1}$  was emission from the line of sight, unrelated to the cloud at  $\sim 150 \text{ km s}^{-1}$ , which matched previous observations of G5. However, the large velocity dispersion of the lower velocity cloud favored it being within the Galactic Center area, as foreground emission from gas in the spiral arms of the galaxy typically has narrow lines ( $< 5 \text{ km s}^{-1}$ ).

#### 4.1. Kinematics

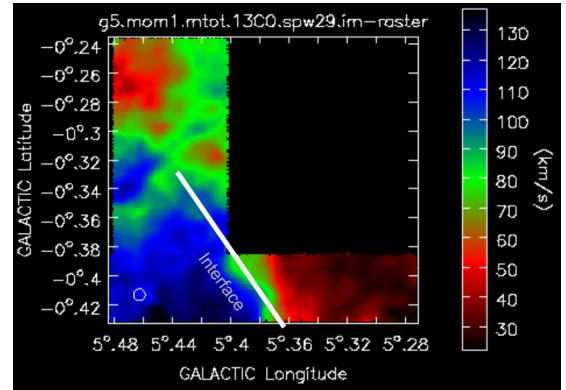


**Figure 6.** Velocity field map in colors opposite the traditional convention, the pixels in blue are more redshifted than the pixels in red. The interface between the two interacting clouds is marked with a white line.

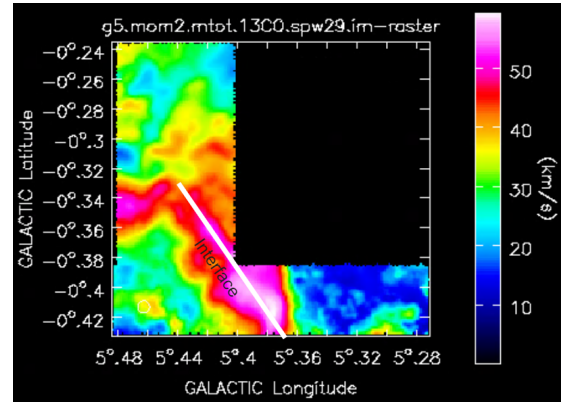


**Figure 7.** Velocity dispersion map in color. The interface between the two interacting clouds is marked with a white line, but is otherwise notable by the enhanced values of the velocity dispersion.

The velocity field of the cloud in Figure 6 shows a gradient between the left  $\sim 150 \text{ km s}^{-1}$  cloud and the right  $\sim 50 \text{ km s}^{-1}$  cloud. This gradient was artificially created by



CASA, as the two clouds overlap in this space, so the program fit a Gaussian between the two clouds' peaks rather than any real emission. The velocity dispersion map in Figure 7 confirms this, showing a sudden broadening from a line width of around  $30 \text{ km s}^{-1}$  to  $50 \text{ km s}^{-1}$  in the same place the gradient appears.

A position-velocity (PV) diagram was created by drawing a line horizontally across the field of G5a for the  $^{12}\text{CO}$  cube, then expanding the width to include the entirety of the field vertically. A PV diagram shows what is going on in velocity space while moving along the 1D position axis, and can give more information on how different sources of emission in a cube are interacting with each other.

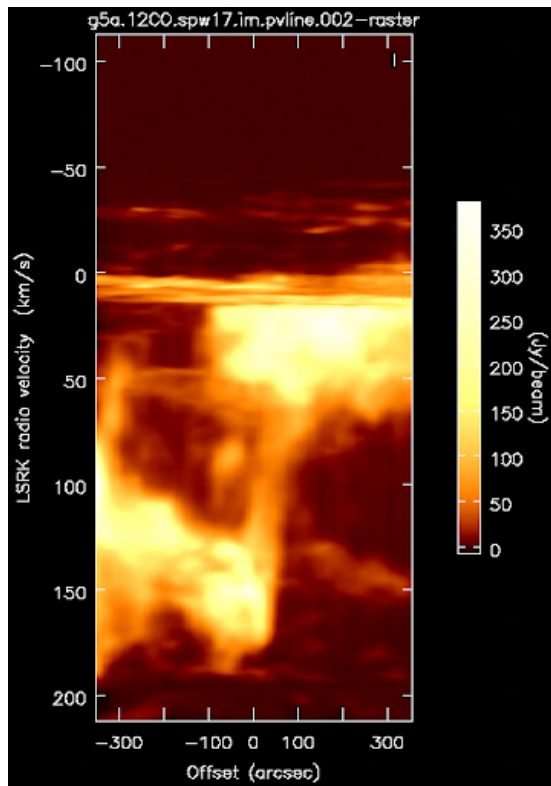


**Figure 8.** Position-Velocity diagram of G5a.

We identified several features in the PV diagram in Figure 8. The first is a cloud with a very wide velocity dispersion on the left side of the field at around  $150 \text{ km s}^{-1}$ , stretching from a position offset of  $-350 \text{ arcsec}$  to around  $50 \text{ arcsec}$ . Another is a second cloud with a wide velocity dispersion on the right side of the field, which is at around  $50 \text{ km s}^{-1}$  but stretches almost to  $0 \text{ km s}^{-1}$ , from a  $-100 \text{ arcsec}$  to  $350 \text{ arcsec}$  offset. Stretching between the two clouds wide in the velocity domain at an offset of around  $50 \text{ arcsec}$  is a velocity bridge. This is direct evidence of a cloud-cloud collision. There is also a clump at  $-50 \text{ arcsec}$  next to the velocity bridge on the PV diagram at around  $75 \text{ km s}^{-1}$ , origins unknown. We identified another feature with an unusually wide velocity from  $30 \text{ km s}^{-1}$  to  $100 \text{ km s}^{-1}$  where it intersects with the  $\sim 150$

$\text{km s}^{-1}$  cloud at around a  $-325 \text{ arcsec}$  offset. While this feature does not seem to directly intersect with the  $\sim 50 \text{ km s}^{-1}$  cloud, there is something at  $\sim 50 \text{ km s}^{-1}$  which it may be interacting with. However, this 'spur' off of the main  $\sim 150 \text{ km s}^{-1}$  cloud has not been conclusively identified. There are also several sources of emission with very narrow velocity dispersion's, which we believe are foreground molecular clouds.

A velocity bridge is a feature in a PV diagram that is wide in velocity space but relatively narrow in position space, and connects two features. In this case, the two features are a cloud at  $\sim 150 \text{ km s}^{-1}$  and a cloud at  $\sim 50 \text{ km s}^{-1}$ , and the velocity bridge is where the two overlap. The  $^{12}\text{CO}$  PV diagram in Figure 8 has a vertical velocity bridge connecting the two clouds. The velocity bridge indicates the two clouds are colliding or otherwise interacting with each other, instead of being coincidentally along the same line of sight where they overlap.

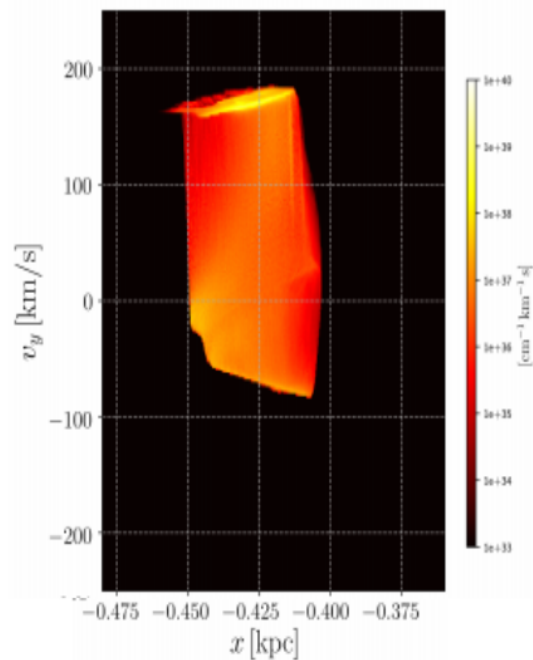


**Figure 9.** An example PV diagram of Sormani et al. (2019)'s model of a cloud-cloud collision.

This cloud collision supports Sormani et al. (2018)'s model of the Milky Way Galactic Center's bar. Sormani's model shows that a cloud going down one of the dust lanes towards the CMZ can overshoot and go past it, hitting the dust lane on the other side of the galaxy (Sormani et al. 2019). Sormani et al. (2019)'s model of a PV diagram of a cloud-cloud collision velocity bridge Figure 9 is similar to the velocity bridge seen in Figure 8. The cloud at  $\sim 50 \text{ km s}^{-1}$  is a molecular cloud that has travelled down the dust lane on the other side of the galaxy, overshoot the CMZ, and is colliding with the  $\sim 150 \text{ km s}^{-1}$  cloud on this side of the galaxy.

#### 4.2. Moment Maps

Integrated intensity, velocity field, and velocity dispersion maps were taken of the two clouds both separately and together using the CASA task `immoments`, specifying the channels. The two clouds slightly overlapped in the middle of the G5a field, but were otherwise separated into either the left (cloud at  $\sim 150 \text{ km s}^{-1}$ ) or right ( $\sim 50 \text{ km s}^{-1}$ ) sides of the field.

#### 4.3. Kinetic Temperature

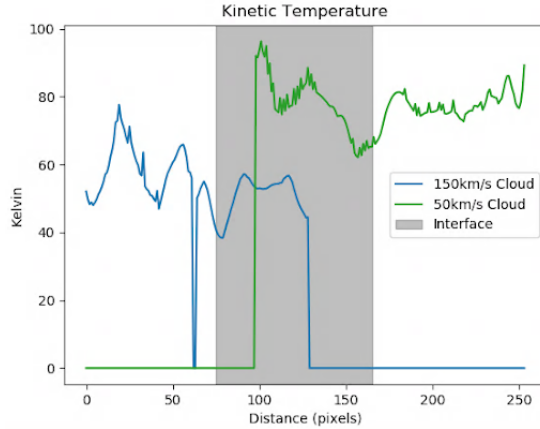


**Figure 10.** Plot of the kinetic temperature slices of the  $\sim 50 \text{ km s}^{-1}$  cloud in green and the  $\sim 150 \text{ km s}^{-1}$  cloud in blue.

The kinetic temperature of the  $\sim 50 \text{ km s}^{-1}$  cloud is around 80K and the  $\sim 150 \text{ km s}^{-1}$  cloud is at 60K in Figure 10. The higher kinetic temperature of the  $\sim 50 \text{ km s}^{-1}$  cloud may mean that it has a longer history of being in the GC than the  $\sim 150 \text{ km s}^{-1}$  cloud. It may have had a close encounter with the CMZ. The  $\sim 50 \text{ km s}^{-1}$  cloud fell into the GC on the other side of the galaxy, heated up during its encounter with the CMZ, and hit the  $\sim 150 \text{ km s}^{-1}$  cloud, which is still in the process of falling into the CMZ.

#### 4.4. Chemical Line Abundance Ratios

The ratios in Figure 11 are different on either side of the interface.

#### 4.5. Shocks

$\text{CH}_3\text{OH}$  ( $4_{22}-3_{12}$ ) traces weak shocks through a medium. Since  $\text{CH}_3\text{OH}$  is an organic molecule, it is thought to form on the surfaces of dust grains. When a weak shock hits these dust grains, it knocks the  $\text{CH}_3\text{OH}$  molecules off and into the gas state, exciting them. The column density abundance ratio of  $\text{CH}_3\text{OH}$  to  $\text{H}_2$  is around  $5e-9$  in Figure 12. Meier & Turner (2005)'s fractional abundance ratio of  $\text{CH}_3\text{OH}$  to  $\text{H}_2$  for extra-galactic bars is  $3e-9$ , an example of an enhanced amount of  $\text{CH}_3\text{OH}$  due to shocks. This suggests that the measured levels of  $\text{CH}_3\text{OH}$  are elevated, meaning that weak shocks travel through this cloud.

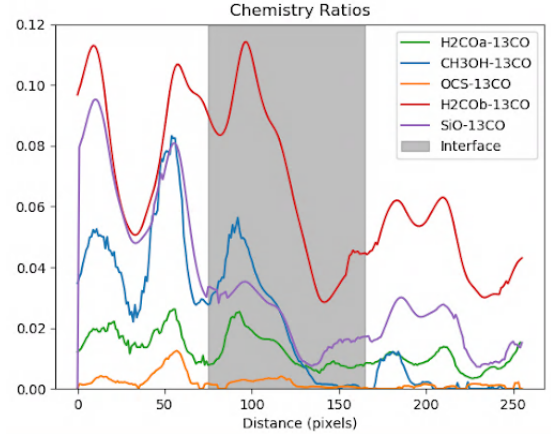


**Figure 11.** Plot of the slices of the ratios between various molecules by  $^{13}\text{CO}$  ( $2-1$ ). Green is  $\text{H}_2\text{CO}$  ( $3_{21}-2_{20}$ ). Blue is  $\text{CH}_3\text{OH}$  ( $4_{22}-3_{12}$ ). Orange is  $\text{OCS}$  ( $18-17$ ). Red is  $\text{H}_2\text{CO}$  ( $3_{03}-2_{02}$ ). Purple is  $\text{SiO}$  ( $5-4$ ). Typical error bars are  $\sim \pm 0.005$ .

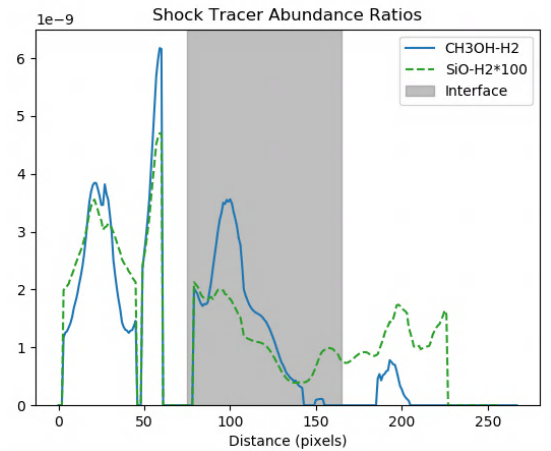


**Figure 12.** Plot of the abundance ratio of the column densities of the shock tracers  $\text{SiO}$  (green) and  $\text{CH}_3\text{OH}$  (blue) to the column density of  $\text{H}_2$ . The  $\text{SiO}$  ratio was augmented by a factor of 100 to make it visible on the plot, and its values are on the order of  $1e-11$ .

$\text{SiO}$  ( $5-4$ ) is a strong shock tracer. Strong shocks are powerful enough to destroy dust grains, causing the solid silicate interior to be exposed to the interstellar medium and turn into a gas. The presence of  $\text{SiO}$  ( $5-4$ ) in this cloud indicates that the cloud has strong shocks travelling through it. If  $\text{SiO}$  is seen at all, then there must be shock velocities above  $20 \text{ km s}^{-1}$  present (Schilke et al. 1997). The column density abundance ratio of  $\text{SiO}$  to  $\text{H}_2$  is around  $5e-11$  in Figure 12.

As the dust lane streaming along the bar arm passes through a shock front, the two clouds were already shocked before interacting. However, the collision between the two clouds caused the amount of shock tracers to be elevated downstream of the shock from the collision, as seen left of the interface in Figure 12.

## 4.6. Opacity

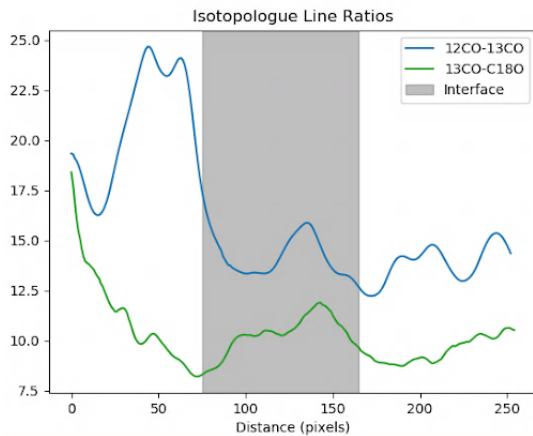


**Figure 13.** Plot of the slice of the isotopologue line ratios. In blue is the ratio between  $^{12}\text{CO}$  (2-1) and  $^{13}\text{CO}$  (2-1). In green is the ratio between  $^{13}\text{CO}$  (2-1) and  $\text{C}^{18}\text{O}$  (2-1).

The isotopologue ratios trace the transparency of the clouds in CO, with a clear difference between the two clouds on either side of the interface in Figure 13. A higher ratio of  $^{12}\text{CO}$  to  $^{13}\text{CO}$  traces where the cloud is translucent in CO. The  $\tau$  values of these clouds varies between 0 to 3, with values of around 10 or above edging on opaque. Both clouds are translucent in CO, with the  $\sim 50 \text{ km s}^{-1}$  cloud being more opaque than the  $\sim 150 \text{ km s}^{-1}$  cloud.

## 5. CONCLUSION

We observed gas flows within the Milky Way’s bar, which are important to study the transfer of gas to the CMZ and how its physical and chemical state changes along the trajectory. We used ALMA to observe two clouds relevant to the bar model of the galaxy, which postulates that the gas flows into the CMZ relative to a bar shaped potential. We found that G5, which we focused on this summer, is composed of two clouds which are colliding with each other. This collision supports Sormani et al. (2019)’s model of gas overshooting the CMZ after travelling down a dust lane and hitting the dust lane on the other side of the bar. Illustrated in Figure 14, the  $\sim 50 \text{ km s}^{-1}$  cloud travelled down the dust lane in red and passed the CMZ in purple. The close encounter with the CMZ warmed the cloud up. It then curved in to hit the blue dust lane on the other side of the galaxy, where the  $\sim 150 \text{ km s}^{-1}$  cloud is falling in towards the CMZ.

## ACKNOWLEDGMENTS

Thank you to NRAO for a fantastic second summer internship. Thank you to Associated Universities, Inc. and the National Science Foundation for funding. Thank you to Yancy Shirley for joining this project and allowing me to continue working on it this school years. Thank you to Anna Kapinska for the summer student teas and for helping me adjust to remote work over this summer.

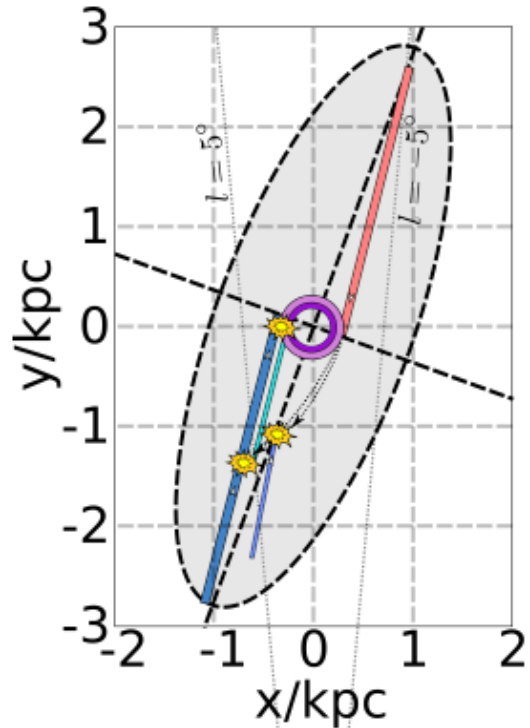


**Figure 14.** Cartoon drawing from Sormani et al. (2019), which shows a top down view of the galaxy. The bursts along the  $l = 5^\circ$  line approximate where G5 is located. The burst on the CMZ is theorized to be the Bania 2 clump.

*Facilities:* Atacama Compact Array, ALMA

*Software:* This research has made use of the following software projects: Astropy (The Astropy Collaboration et al. 2018), Matplotlib (Hunter 2007), NumPy, SciPy (Oliphant 2007), Imfit, IPython (Pérez & Granger 2007), CASA (McMullin et al. 2007), and the NASA’s Astrophysics Data System.

## APPENDIX

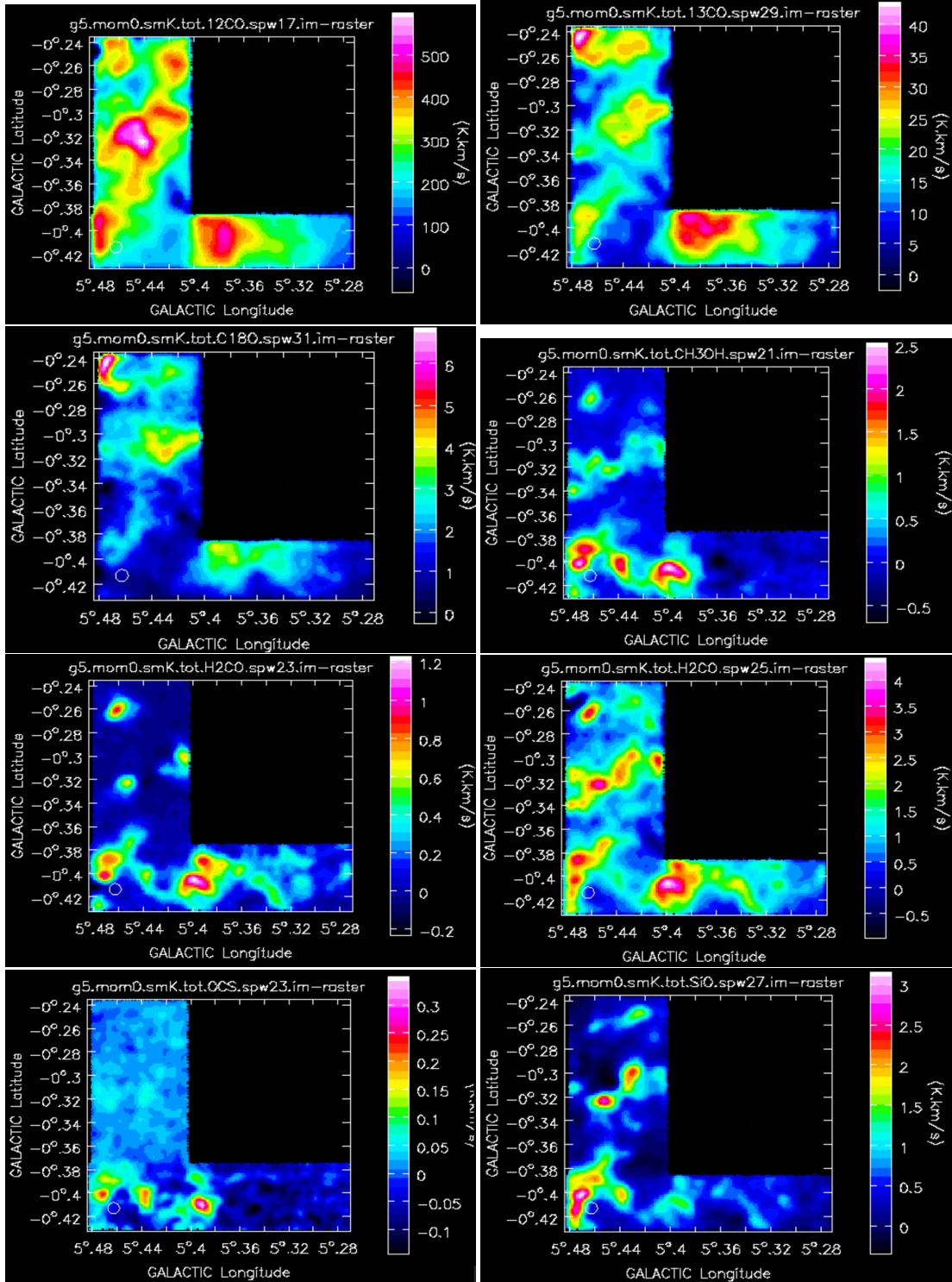


**Figure 15.** Integrated Intensity maps of the surveyed region of G5. First row: first image is  $^{12}CO$  (2-1), second image is  $^{13}CO$  (2-1). Second row:  $C^{18}O$  (2-1),  $CH_3OH$  (4<sub>22</sub>-3<sub>12</sub>). Third row:  $H_2CO$  (3<sub>22</sub>-2<sub>21</sub>),  $H_2CO$  (3<sub>03</sub>-2<sub>02</sub>). Fourth row: OCS (18-17), SiO (5-4).



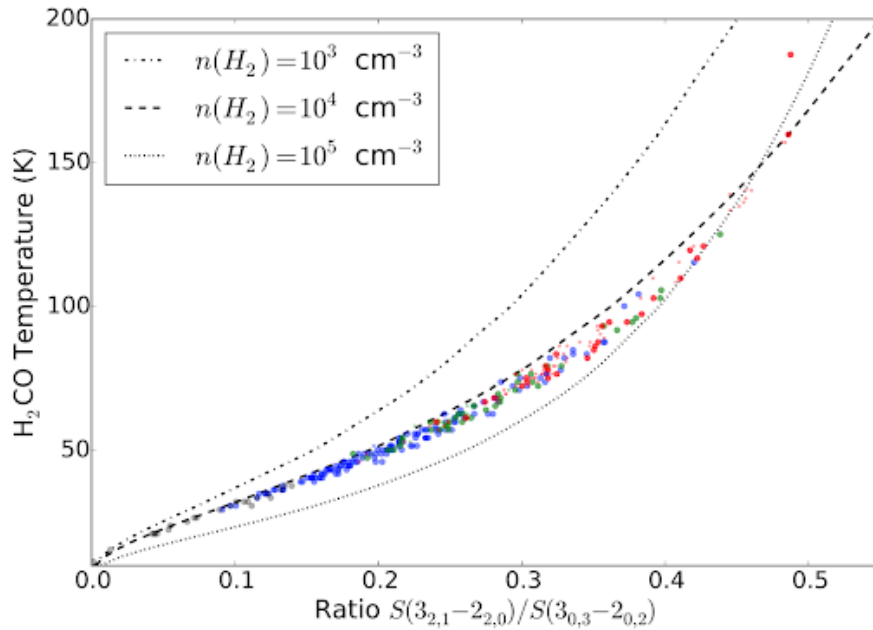


**Figure 16.** Plot from Ginsburg et al. (2016), showing the relationship between the ratio of the H<sub>2</sub>CO lines and the kinetic temperature for warm clouds.

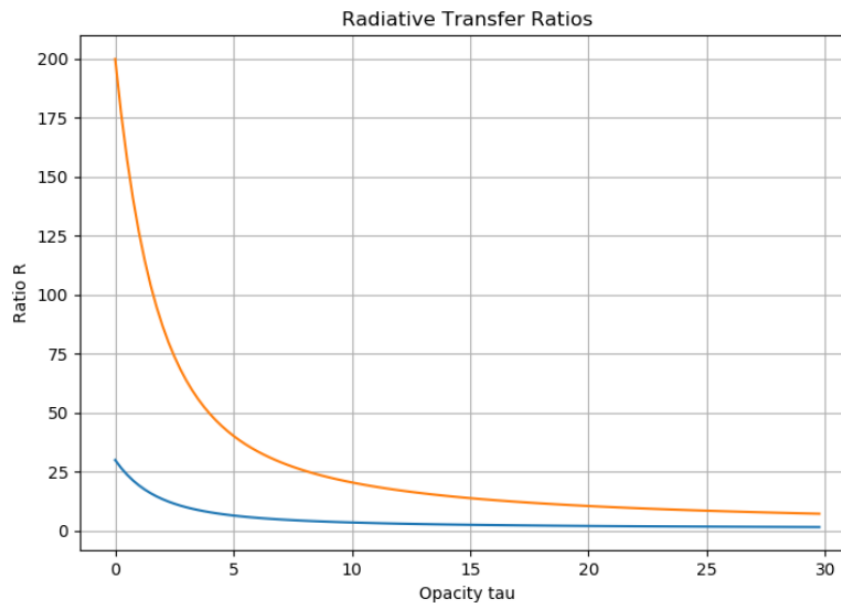


**Figure 17.** This is two overlaid plots of Equation 2 with isotropic ratio values of 30 and 200. The blue line is for <sup>13</sup>CO and the orange is for C<sup>18</sup>O. The ratios of the integrated intensity of these isotopologues relative to that of <sup>12</sup>CO give the ratio on the vertical axis, which can then be used to approximate  $\tau$ .

#### REFERENCES

Bania, T. M., Stark, A. A., & Heiligman, G. M. 1986, ApJ, 307, 350, doi: [10.1086/164422](https://doi.org/10.1086/164422)  
 Ginsburg, A., Henkel, C., Ao, Y., et al. 2016, A&A, 586, A50, doi: [10.1051/0004-6361/201526100](https://doi.org/10.1051/0004-6361/201526100)

Gramze, S., Ott, J., Meier, D., & Svoboda, B. 2020, in American Astronomical Society Meeting Abstracts, American Astronomical Society Meeting Abstracts, 310.05

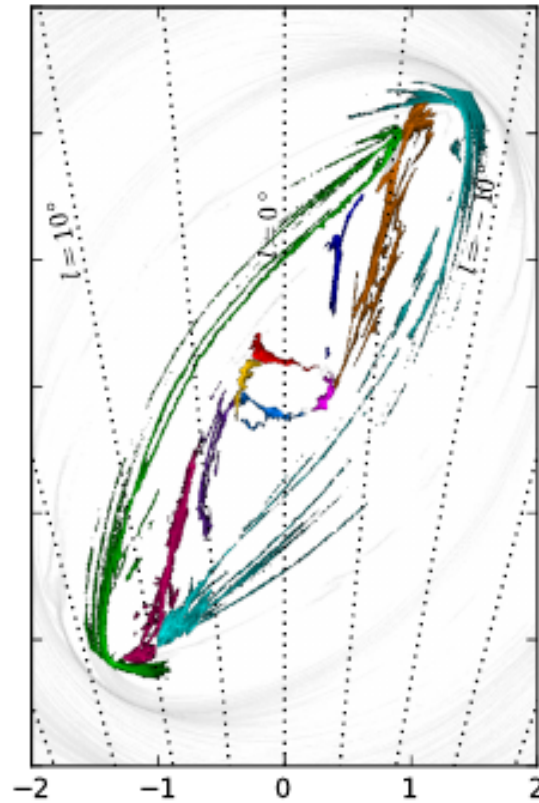


**Figure 18.** A snapshot of a simulation of a top down view of the Milky Way galaxy from Sormani et al. (2018).

- Hunter, J. D. 2007, *Computing In Science & Engineering*, 9, 90, doi: [10.1109/MCSE.2007.55](https://doi.org/10.1109/MCSE.2007.55)
- Longmore, S. N., Walsh, A. J., Purcell, C. R., et al. 2017, *MNRAS*, 470, 1462, doi: [10.1093/mnras/stx1226](https://doi.org/10.1093/mnras/stx1226)
- Mangum, J. G., & Shirley, Y. L. 2015, *PASP*, 127, 266, doi: [10.1086/680323](https://doi.org/10.1086/680323)
- McMullin, J. P., Waters, B., Schiebel, D., Young, W., & Golap, K. 2007, in *Astronomical Society of the Pacific Conference Series*, Vol. 376, *Astronomical Data Analysis Software and Systems XVI*, ed. R. A. Shaw, F. Hill, & D. J. Bell, 127
- Meier, D. S., & Turner, J. L. 2005, *ApJ*, 618, 259, doi: [10.1086/426499](https://doi.org/10.1086/426499)
- Morris, M., & Serabyn, E. 1996, *ARA&A*, 34, 645, doi: [10.1146/annurev.astro.34.1.645](https://doi.org/10.1146/annurev.astro.34.1.645)
- Oliphant, T. E. 2007, *Computing in Science & Engineering*, 9
- Pérez, F., & Granger, B. E. 2007, *Computing in Science & Engineering*, 9
- Purcell, C. R., Longmore, S. N., Walsh, A. J., et al. 2012, *MNRAS*, 426, 1972, doi: [10.1111/j.1365-2966.2012.21800.x](https://doi.org/10.1111/j.1365-2966.2012.21800.x)
- Schilke, P., Walmsley, C. M., Pineau des Forets, G., & Flower, D. R. 1997, *A&A*, 321, 293
- Sormani, M. C., Binney, J., & Magorrian, J. 2015, *MNRAS*, 449, 2421, doi: [10.1093/mnras/stv441](https://doi.org/10.1093/mnras/stv441)
- Sormani, M. C., Treß, R. G., Ridley, M., et al. 2018, *MNRAS*, 475, 2383, doi: [10.1093/mnras/stx3258](https://doi.org/10.1093/mnras/stx3258)
- Sormani, M. C., Treß, R. G., Glover, S. C. O., et al. 2019, *MNRAS*, 1994, doi: [10.1093/mnras/stz2054](https://doi.org/10.1093/mnras/stz2054)
- Strong, A. W., Bloemen, J. B. G. M., Dame, T. M., et al. 1988, *A&A*, 207, 1
- The Astropy Collaboration, Price-Whelan, A. M., Sipőcz, B. M., et al. 2018, *AJ*, 156, 123, doi: [10.3847/1538-3881/aabc4f](https://doi.org/10.3847/1538-3881/aabc4f)
- van der Tak, F. F. S., Black, J. H., Schöier, F. L., Jansen, D. J., & van Dishoeck, E. F. 2007, *A&A*, 468, 627, doi: [10.1051/0004-6361:20066820](https://doi.org/10.1051/0004-6361:20066820)
- Walsh, A. J., Breen, S. L., Britton, T., et al. 2011, *MNRAS*, 416, 1764, doi: [10.1111/j.1365-2966.2011.19115.x](https://doi.org/10.1111/j.1365-2966.2011.19115.x)